

Chapter 8

Pseudogapped Crossover Theory

8.1 Introduction

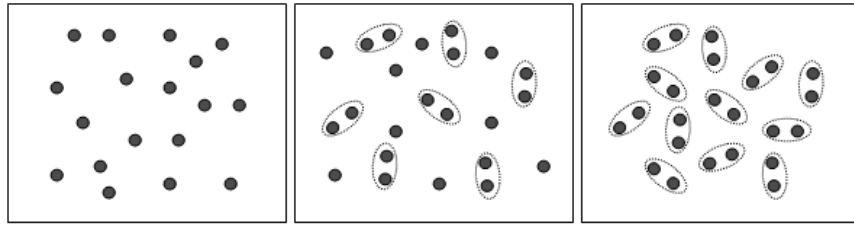


Figure 8.1: For weak coupling (left) the normal phase consists of interacting fermions. As the coupling is increased (middle) preformed pairs may appear. At lower temperatures these pairs may become coherent resulting in a superfluid transition. For strong couplings (right), the system is composed only of fermion pairs which may condense at low enough temperature.

The resonant crossover work discussed in the previous chapter introduced the idea of preformed pairs which form above the critical temperature for superfluidity. One would expect that the presence of these pairs would alter the nature of the gas from that of a simple degenerate Fermi gas. For instance, just as the presence of coherent, Cooper pairing modifies the energy spectrum below T_c , leading to the effects witnessed in superfluidity, we might expect that incoherent pairs might also modify the energy spectrum leading to other novel phenomena (see Fig. (8.1)). These above T_c effects are often referred to as “pseudogap” effects and the region between superfluidity and a

normal Fermi gas (the temperature noting this second phase is often referred to as T^*) is known as the pseudogap region.

Unfortunately, although beginning to account for the presence of preformed pairs, the work of the previous section has several shortcomings [90, 91], most notably, it does not account for the effects of the pseudogapped region above T_c . In fact, the form of the pair propagator given in Eq. (7.12) treats the pairs as composed of two free fermions uncoupled from the medium (i.e., there is no self-energy term in the propagators). In this section we wish to account for pseudogap effects by adapting a theory originally proposed by Kadanoff and Martin [92] and extended to account for high- T_c effects by several authors [93, 94, 95]. An alternative approach to including these pseudogap effects, in a non-resonant system, may be found in reference [96], although we feel this approach may overemphasize the importance of these contributions.

Although, at first it may appear quite different, the mode coupling approach we are about to present [97] is quite similar to the dynamical approach followed in Chapter 5. Now, however, higher-order correlations are to be accounted for. These correlations will result in the process of pair formation and will lead to the pseudogapped behavior we wish to incorporate.

8.2 Dynamical Green's function method

We begin with a discussion of dynamical Green's functions [98]. One method to solve for the single-particle Green's function, which encompasses all the information of a system, is to derive an infinite hierarchy of dynamical equations and then to truncate, or decouple, those equations at a given order. To see how this may be done we first define the single-particle Green's function:

$$\begin{aligned} G^\alpha(\mathbf{x}_1 t_1, \mathbf{x}_{1'} t_{1'}) &= -i \left\langle T(\psi_\alpha(\mathbf{x}_1, t_1) \psi_\alpha^\dagger(\mathbf{x}_{1'}, t_{1'})) \right\rangle \\ &= -i \left(\Theta(t_1 - t_{1'}) \left\langle \psi_\alpha(\mathbf{x}_1, t_1) \psi_\alpha^\dagger(\mathbf{x}_{1'}, t_{1'}) \right\rangle - \Theta(t_{1'} - t_1) \left\langle \psi_\alpha^\dagger(\mathbf{x}_{1'}, t_{1'}) \psi_\alpha(\mathbf{x}_1, t_1) \right\rangle \right), \end{aligned} \quad (8.1)$$

where $\psi_\alpha^\dagger(\mathbf{x}, t)$ ($\psi_\alpha(\mathbf{x}, t)$) creates(destroys) a particle of spin index α at position x at time t and $\Theta(t_1 - t'_1)$ is the step function defined as:

$$\Theta(t - t') = \begin{cases} 0, & t < t' \\ 1, & t > t' \end{cases}. \quad (8.2)$$

The inclusion of the step function in the second line of Eq. (8.1) defines the time ordering T in the first. Higher-order Green's functions may be defined in a similar way

$$\begin{aligned} G_2^{\alpha\beta}(\mathbf{x}_1 t_1, \mathbf{x}_2 t_2; \mathbf{x}_1' t_1', \mathbf{x}_2' t_2') &= (-i)^2 \langle \psi_\alpha(\mathbf{x}_1, t_1) \psi_\beta(\mathbf{x}_2, t_2) \psi_\beta^\dagger(\mathbf{x}_2', t_2') \psi_\alpha^\dagger(\mathbf{x}_1', t_1') \rangle \\ G_3^{\alpha\beta\gamma}(\mathbf{x}_1 t_1, \mathbf{x}_2 t_2, \mathbf{x}_3 t_3; \mathbf{x}_1' t_1', \mathbf{x}_2' t_2', \mathbf{x}_3' t_3') &= \dots \text{etc.} \end{aligned} \quad (8.3)$$

We may also define the noninteracting Green's function by the useful relation

$$G_0^{-1}(\mathbf{x}_1, t_1) G_0(\mathbf{x}_1 t_1, \mathbf{x}_1' t_1') = \delta(\mathbf{x}_1 t_1, \mathbf{x}_1' t_1'), \quad (8.4)$$

where we have suppressed the spin indexes in this last formula.

We would now like to generate a set of equations from which we may solve for the single-particle Green's function describing the interacting system. In what follows, we will focus on a two component system of interacting fermions and begin by defining the single-channel Hamiltonian ($\hbar = 1$):

$$H_A = \sum_\alpha \int d^3\mathbf{x} \psi_\alpha^\dagger(\mathbf{x}) \left(-\frac{\nabla^2}{2m}\right) \psi_\alpha(\mathbf{x}) + \int d^3\mathbf{x} d^3\mathbf{x}' \psi_\uparrow^\dagger(\mathbf{x}) \psi_\downarrow^\dagger(\mathbf{x}') U(\mathbf{x}, \mathbf{x}') \psi_\downarrow(\mathbf{x}') \psi_\uparrow(\mathbf{x}), \quad (8.5)$$

where α runs over all spin components. An entire hierarchy of dynamical equations can be generated starting with the equation of motion for the field operator

$$i \frac{\partial}{\partial t} \psi_\alpha(\mathbf{x}t) = -\frac{\nabla^2}{2m} \psi_\alpha(\mathbf{x}t) + \int d^3\bar{\mathbf{x}} U(\mathbf{x}, \bar{\mathbf{x}}) \psi_\beta^\dagger(\bar{\mathbf{x}}t) \psi_\beta(\bar{\mathbf{x}}t) \psi_\alpha(\mathbf{x}t). \quad (8.6)$$

For example, the equation of motion for the first order Green's function is

$$\begin{aligned} \left(i \frac{\partial}{\partial t_1} + \frac{\nabla_1^2}{2m} \right) G^\alpha(\mathbf{x}_1 t_1, \mathbf{x}_1' t_1') &= \delta^3(\mathbf{x}_1 - \mathbf{x}_1') \delta(t_1 - t_1') \\ &- i \int d^3\bar{\mathbf{x}} U(\mathbf{x}_1, \bar{\mathbf{x}}) G_2^{\alpha\beta}(\mathbf{x}_1 t_1, \bar{\mathbf{x}} t_1; \mathbf{x}_1' t_1', \bar{\mathbf{x}} t_1'). \end{aligned} \quad (8.7)$$

Here we have introduced the argument t^+ to denote an infinitesimal positive time above t so that we may cast the equation in the above form. Likewise, we may solve for the equation of motion of the second order Green's function

$$\left(i\frac{\partial}{\partial t_1} + \frac{\nabla_1^2}{2m}\right) G_2^{\alpha\beta}(\mathbf{x}_1 t_1, \mathbf{x}_2 t_2; \mathbf{x}_1' t_1', \mathbf{x}_2' t_2') = \delta^3(\mathbf{x}_1 - \mathbf{x}_1') \delta(t_1 - t_1') G^\alpha(\mathbf{x}_2 t_2, \mathbf{x}_2' t_2') - i \int d\bar{\mathbf{x}}^3 U(\mathbf{x}_1, \bar{\mathbf{x}}) G_3^{\alpha\beta\beta}(\mathbf{x}_1 t_1, \mathbf{x}_2 t_2, \bar{\mathbf{x}} t_1; \mathbf{x}_1' t_1', \mathbf{x}_2' t_2', \bar{\mathbf{x}} t_1^+). \quad (8.8)$$

This procedure, of course, may be continued ad nauseam, but, in order to make use of these equations, the hierarchy will need to be truncated at a given order. The method chosen for performing this truncation sets the level of approximation at which we are calculating the single-particle Green's function. The next section discusses various ways in which this may be done.

8.3 Truncation of the equations of motion

For the work that follows in this chapter, we will chose to truncate this hierarchy of equations at the order of the two-particle Green's function G_2 . We must, therefore, decide how to properly account for the coupling of Eq. (8.8) to the three-particle Green's function G_3 . For the moment, we will not consider anomalous correlations, but instead will focus on the region $T > T_c$ where we assume only conserving correlations are relevant. Under this condition, and the assumption that we have an equal mixture of spin states, we may keep only correlations which conserve both spin and number. A lowest order approximation of this type would be to factorize G_3 as:

$$G_3^{\alpha\beta\beta}(1, 2, \bar{1}; 1'2', \bar{1}^+) \approx G(1, 1')G(2, 2')G(\bar{1}, \bar{1}^+) - G(1, 1')G(2, \bar{1}^+)G(\bar{1}, 2'). \quad (8.9)$$

We have introduced the 4-vector notation $(1) = (\mathbf{x}, t)$ for convenience in writing the various correlation functions. The above factorization is just the usual Hartree-Fock (HF) approximation encountered throughout this thesis and neglects the effects of all but pairwise correlations. This is the level of approximation used in Chapter 5, however,

we would like to go beyond this approximation to begin to account for higher order correlations between the particles.

A next order factorization would involve writing G_3 in terms of factors of GG_2 and GGG . This is known as a cumulant expansion and may be written [92]:

$$\begin{aligned}
 G_3^{\alpha\beta\beta}(1, 2, \bar{1}; 1', 2', \bar{1}^+) &\approx G(2, 2')G_2^{\alpha\beta}(1, \bar{1}; 1', \bar{1}^+) + G(\bar{1}, \bar{1}^+)G_2^{\alpha\beta}(1, 2; 1', 2') \quad (8.10) \\
 &- G(2, \bar{1}^+)G_2^{\alpha\beta}(1, \bar{1}; 1', 2') - G(\bar{1}, 2')G_2^{\alpha\beta}(1, 2; 1', \bar{1}^+) \\
 &- G(1, 1')G(2, 2')G(\bar{1}, \bar{1}^+) + G(1, 1')G(2, \bar{1}^+)G(\bar{1}, 2').
 \end{aligned}$$

In the above equation we have dropped the correlated component of $G(1, 1')G_2^{\beta\beta}(2, \bar{1}; 2', \bar{1}^+)$ since only particles of opposite spin may collide. Notice that if we were to Wick expand the various G_2 functions we would indeed get the HF result of Eq. (8.9). Physically, the form for the three-particle Green's function G_3 , which we have written, describes the interaction of three particles taking into account that two of the particles may be correlated during the interaction process and neglects all higher order correlations (see Fig. 8.2).

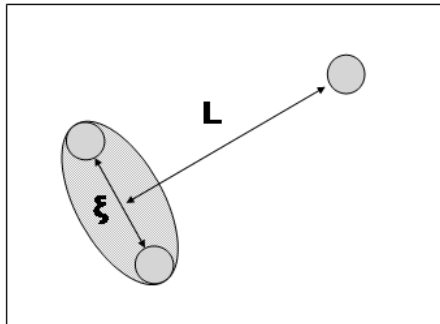


Figure 8.2: The factorization performed in Eq. (8.10) approximates the collisions of three particles by the scattering of a particle off a correlated pair. The approximation should remain valid, even for strong pair-correlations, so long as the pair size ξ remains smaller than the mean inter-particle spacing L .

Substituting the form of G_3 given by Eq. (8.10) into Eq. (8.8), we may write Eq. (8.8)

as:

$$\begin{aligned} \left(i\frac{\partial}{\partial t_1} + \frac{\nabla_1^2}{2m}\right) L_2^{\alpha\beta}(1, 2; 1', 2') &= -i \int d\bar{1} U(1, \bar{1}) [G(\bar{1}, \bar{1}^+) L_2^{\alpha\beta}(1, 2; 1', 2')] \\ &\quad - G(2, \bar{1}^+) G_2^{\alpha\beta}(1, \bar{1}; 1', 2') - G(\bar{1}, 2') L_2^{\alpha\beta}(1, 2; 1', \bar{1}^+), \end{aligned} \quad (8.11)$$

where I have made use of Eqs. (8.4) and (8.7), and have introduced the notation

$$L_2^{\alpha\beta}(1, 2; 1', 2') = G_2^{\alpha\beta}(1, 2; 1', 2')' - G(1, 1') G(2, 2'). \quad (8.12)$$

This new function L_2 accounts for the correlated part of the Green's function G_2 . Now, by absorbing the shift given by the first term on the right hand side of Eq. (8.11) into the definition of the free-particle Green's function, we may simplify things even further:

$$\tilde{G}_0^{-1}(1) L_2^{\alpha\beta}(1, 2; 1', 2') = i \int d\bar{1} U(1, \bar{1}) [G(2, \bar{1}^+) G_2^{\alpha\beta}(1, \bar{1}; 1', 2') + G(\bar{1}, 2') L_2^{\alpha\beta}(1, 2; 1', \bar{1}^+)], \quad (8.13)$$

where

$$\tilde{G}_0^{-1}(1) = G_0^{-1}(1) + i \int d\bar{1} U(1, \bar{1}) G(\bar{1}, \bar{1}^+), \quad (8.14)$$

and we have identified the free particle Green's function

$$G_0^{-1}(1) = \left(i\frac{\partial}{\partial t_1} + \frac{\nabla_1^2}{2m}\right). \quad (8.15)$$

The first term on the right hand side of Eq. (8.13) will produce a series of ladder diagrams. The second term, which represents all the multiple scattering events where the interaction lines cross, we will drop. It is hoped that the ladder summation will account for the dominant processes involved. These statements might be made clearer by representing Eq. (8.13) diagrammatically, as shown in Fig. 8.3.

The above approximation, as noted in the caption of Fig. 8.2, should remain valid in the regime where the correlation length between pairs of atoms remains smaller than the mean inter-particle spacing. This is just the sort of term that we are interested in since it introduces the process of an atom scattering off a correlated pair, in analogy to

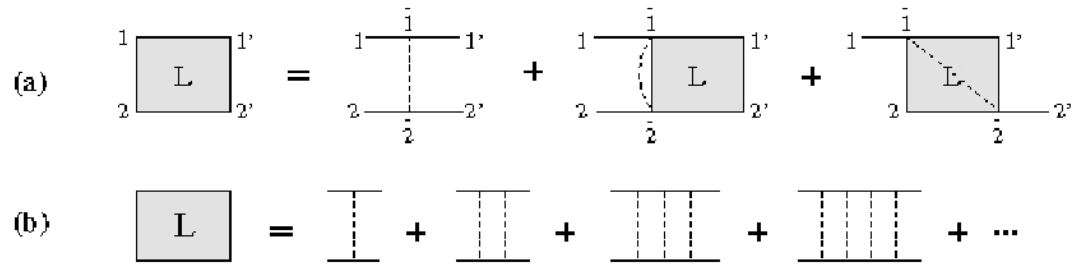


Figure 8.3: (a) Diagrammatic representation of Eq. 8.13. The thin lines denote the free Green's functions \tilde{G}_0 , thick lines are the full Green's functions G , and dotted lines represent the interaction U . (b) Diagrammatic representation of the resulting ladder summation.

the scattering of an atom and a molecule. The final result is an integral equation for G_2 which may be written as:

$$G_2^{\alpha\beta}(1, 2; 1', 2') = G(1, 1')G(2, 2') + i \int d\bar{1} d\bar{2} \tilde{G}_0(1, \bar{1})U(\bar{1}, \bar{2})G(2, \bar{2})G_2^{\alpha\beta}(\bar{1}, \bar{2}; 1', 2') \quad (8.16)$$

We have written the above equation in this form to illustrate the extension from the Hartree-Fock approach (notice the lowest order term is just the HF result).

8.4 Extension to resonant Hamiltonian

Equation (8.16) was derived for the single-channel Hamiltonian of Eq. (8.5). We would like to extend these results to account for a molecular channel so, as we have done earlier, we include the resonant molecular processes in the hamiltonian:

$$H_B = \int d^3x \varphi_m^\dagger(\mathbf{x}) \left(-\frac{\nabla^2}{4m} + \nu \right) \varphi_m(\mathbf{x}) + \int d^3x d^3x' \left[\varphi_m^\dagger\left(\frac{\mathbf{x} + \mathbf{x}'}{2}\right) g(\mathbf{x} - \mathbf{x}') \psi_\downarrow(\mathbf{x}) \psi_\uparrow(\mathbf{x}) + h.c. \right]. \quad (8.17)$$

In analogy to the previous section, we first define the molecular Green's function

$$D(\mathbf{x}_1 t_1, \mathbf{x}_1' t_1') = -i \langle T(\varphi_m(\mathbf{x}_1, t_1) \varphi_m^\dagger(\mathbf{x}_1', t_1')) \rangle. \quad (8.18)$$

We could likewise define higher order molecular Green's functions in much the same way as we defined the higher order Fermi Green's functions. For the moment, let us only introduce this definition. What's more, we must now write down what we may refer to simply as "mixed" Green's function

$$M(\mathbf{x}_1 t_1, \mathbf{x}_2 t_2; \mathbf{x}_{1'} t_{1'}) = (-i)^2 \langle T(\psi_\uparrow(\mathbf{x}_1, t_1) \psi_\downarrow(\mathbf{x}_2, t_2) \varphi_m^\dagger(\mathbf{x}_{1'}, t_{1'})) \rangle, \quad (8.19)$$

which accounts for correlations between atoms and molecules. We will quickly see that these two definitions are all we will need.

Using the full resonant Hamiltonian we may derive the equation of motion for the molecular field operator as:

$$i \frac{\partial}{\partial t} \varphi_m(\mathbf{x}t) = \frac{-\nabla^2}{4m} \varphi_m(\mathbf{x}t) + \int d^3 \bar{x} g(\mathbf{x}, \bar{\mathbf{x}}) \psi_\downarrow(\bar{\mathbf{x}}) \psi_\uparrow(\mathbf{x}) \quad (8.20)$$

From this equation, naturally, follows the equation for the lowest order molecular Green's function

$$\begin{aligned} \left(i \frac{\partial}{\partial t_1} + \frac{\nabla_1^2}{4m} \right) D(\mathbf{x}_1 t_1, \mathbf{x}_{1'} t_{1'}) &= \delta^3(\mathbf{x}_1 - \mathbf{x}_{1'}) \delta(t_1 - t_{1'}) \\ &- i \int d^3 \bar{x} g(\mathbf{x}_1, \bar{\mathbf{x}}) M(\bar{\mathbf{x}} t_1, \bar{\mathbf{x}} t_{1'}; \mathbf{x}_{1'} t_{1'}). \end{aligned} \quad (8.21)$$

From Eq. (8.21) we see that the coupling to higher order terms is through the mixed function M . If we now look at the equation of motion for the mixed Green's function, once again making use of Eq. (8.20), we find:

$$\left(i \frac{\partial}{\partial t_1} + \frac{\nabla_1^2}{4m} \right) M(\mathbf{x}_1 t_1, \mathbf{x}_1 t_1; \mathbf{x}_{1'} t_{1'}) = - \int d^3 \bar{x} g(\mathbf{x}_1, \bar{\mathbf{x}}) G_2^{\alpha\beta}(\mathbf{x}_1 t_1, \bar{\mathbf{x}} t_1; \mathbf{x}_{1'} t_{1'}, \bar{\mathbf{x}} t_1^\dagger). \quad (8.22)$$

Notice that this equation can be solved for M and plugged into our earlier Eq. (8.21) to derive a relation for the full molecular Green's function in terms of G_2 . From this result we find that the modification to Eq. (8.7) is equivalent to the substitution

$$V_{eff}(\mathbf{x}, \mathbf{x}') = U(\mathbf{x}, \mathbf{x}') - D_0(\mathbf{x}, \mathbf{x}') g(\mathbf{x}, \mathbf{x}')^2, \quad (8.23)$$

where we have defined the free molecular Green's function

$$D_0^{-1} = i \frac{\partial}{\partial t_1} + \frac{\nabla_1^2}{4m}. \quad (8.24)$$

Therefore, as far as the fermionic part of our problem is concerned, the only modification that the resonant part of the Hamiltonian incurs is that the fermions now interact through the effective potential V_{eff} . This is an equivalent result as to what we found in Chapter 7 (see Eq. (7.8)) in our adaptation of the NSR approach to the resonant molecular system.

8.5 Self-energy and definition of the t-matrix

It is much easier to work in momentum space since the integral equations found in the previous section convert into algebraic equations. From Eqs. (8.7) and (8.16) we may immediately write an equation for the full Green's function

$$G = \tilde{G}_0 + i\tilde{G}_0 \frac{\chi V_{eff}}{1 + \xi} \tilde{G}_0 G, \quad (8.25)$$

where we define the pair susceptibility to be

$$\chi = -iV_{eff}\tilde{G}_0 G. \quad (8.26)$$

This should be compared to the resonant NSR susceptibility of Eq. (7.12) which is composed of two free propagators. The inclusion of the fully dressed Green's function G in the susceptibility is one of the major extensions of this approach since the presence of a self-energy couples the pairs to the medium.

In deriving Eq. (8.25) we have made the minor simplification of replacing one GG pair, appearing in the numerator, with a $\tilde{G}_0 G$ pair. This is equivalent to replacing the upper, left-most, full Green's function arm, in the ladder diagram of Fig. 8.3, with a bare Green's function \tilde{G}_0 . This results in the irreducible self-energy:

$$\Sigma = \tilde{G}_0^{-1} - G^{-1} = i \frac{\chi V_{eff}}{1 + \xi} \tilde{G}_0. \quad (8.27)$$

To further simplify the equations, we make an approximation in how we incorporate the Hartree shift of the free Green's function (as given in Eq. 8.14), that is, we put it back into the self-energy at lowest order and replace \tilde{G}_0 with G_0 . This results in the following equation for the self-energy.

$$\Sigma = G_0^{-1} - G^{-1} = \frac{-iV_{eff}G_0}{1 + \chi} \equiv tG_0. \quad (8.28)$$

This last equation gives a general definition for the t-matrix t . The t-matrix will prove to be a useful quantity since it may be used to define the critical point of superfluidity. This statement, known as the Thouless criterion, states that the onset of superfluidity occurs as an instability in the t-matrix or:

$$t^{-1} = 0. \quad (8.29)$$

We will often refer back to this condition in the following section.

8.6 Foundations of a pseudogapped resonant crossover theory

Before moving to a discussion on the application of sections 8.3-8.5 to the superfluid regime, $T < T_c$, let us first summarize the major results which we have found. To this end, we begin with the Hamiltonian describing the atomic resonance system written in momentum space:

$$\begin{aligned} H - \mu N &= \sum_{\mathbf{k}, \sigma} \epsilon_{\mathbf{k}} a_{\mathbf{k}, \sigma}^\dagger a_{\mathbf{k}, \sigma} + \sum_{\mathbf{q}} (\epsilon_{\mathbf{q}}^m + \nu) b_{\mathbf{q}}^\dagger b_{\mathbf{q}} \\ &+ \sum_{\mathbf{q}, \mathbf{k}, \mathbf{k}'} U(\mathbf{k}, \mathbf{k}') a_{\mathbf{q}/2+\mathbf{k}, \uparrow}^\dagger a_{\mathbf{q}/2-\mathbf{k}, \downarrow}^\dagger a_{\mathbf{q}/2-\mathbf{k}', \downarrow} a_{\mathbf{q}/2+\mathbf{k}', \uparrow} \\ &+ \sum_{\mathbf{q}, \mathbf{k}} \left(g(\mathbf{k}) b_{\mathbf{q}}^\dagger a_{\mathbf{q}/2-\mathbf{k}, \downarrow} a_{\mathbf{q}/2+\mathbf{k}, \uparrow} + \text{h.c.} \right). \end{aligned} \quad (8.30)$$

The above Hamiltonian, which should be familiar to the reader by now, contains both fermions $a_{\mathbf{k}, \sigma}$ and (spinless) bosonic molecules $b_{\mathbf{q}}$ (the sum in σ runs over both spin states $\{\uparrow, \downarrow\}$). The free dispersion relations for fermions and bosons are given by:

$$\epsilon_{\mathbf{k}} = k^2/2m - \mu \quad \text{and} \quad \epsilon_{\mathbf{q}}^m = q^2/2M - 2\mu, \quad (8.31)$$

respectively, where we assume an equal proportion of spins $\mu_\uparrow = \mu_\downarrow$ and the mass of the boson is just twice that of the a single fermion $M = 2m$. Once again, ν is the detuning of the resonance state.

Until this point we have solely made use of contact potentials within all our many-body theories. However, for the work that follows, we will use a set of Gaussian, separable potentials. For instance, we set the direct s -wave interaction $U(\mathbf{k}, \mathbf{k}') = U\varphi_{\mathbf{k}}\varphi_{\mathbf{k}'}$ and the Feshbach coupling $g(\mathbf{k}) = g\varphi_{\mathbf{k}}$, where the function $\varphi_{\mathbf{k}}^2 = \exp\{-(k/K_c)^2\}$ provides a momentum cutoff K_c (note, we have set $\hbar = k_B = 1$). This choice of potentials, although at the same level of accuracy as the contact potential model, proves more amenable to our later numerical calculations and may be renormalized by the relations given in Appendix A.3.

We have recognized the relevant propagators for the resonant system. These are the propagator for the fermion pairs $t(Q)$, for the molecular bosons $D(Q)$, and for the individual fermions $G(Q)$. As we have seen, the interaction effects induced by the molecular field are equivalent to an effective pairing interaction. For the separable Gaussian potentials we have introduced, this may be written as

$$\tilde{g}_{eff}(Q, K, K') = g_{eff}(Q)\varphi_{\mathbf{k}}\varphi_{\mathbf{k}'}, \quad (8.32)$$

with

$$g_{eff}(Q) \equiv U + g^2 D_0(Q), \quad (8.33)$$

where $D_0(Q) \equiv 1/[i\Omega_n - q^2/2M - \nu + 2\mu]$ is the non-interacting molecular boson propagator (see Eq. (8.23)).

We have also found a particular form for the fermion pair-susceptibility, or the pair propagator $\chi(Q)$:

$$\chi(Q) = \sum_K G(K)G_0(Q - K)\varphi_{\mathbf{k}-\mathbf{q}/2}^2, \quad (8.34)$$

provided that the fermion self-energy appearing in the dressed propagator G is

$$\Sigma(K) = \sum_Q t(Q)G_0(Q-K)\varphi_{\mathbf{k}-\mathbf{q}/2}^2. \quad (8.35)$$

Here and throughout, we take the convention $\sum_K \equiv T \sum_{\omega_n} \sum_{\mathbf{k}}$, where K is a 4-vector of wavenumber \mathbf{k} and Matsubara frequency ω_n . The form of Eq. (8.34) will allow us to account for non-condensed atom pairs and, in contrast to that found by NSR, accounts for a *dressed* fermion pair.

8.7 Extension below T_c and the appearance of an order parameter

So far we have only considered the region $T > T_c$ and would now like to extend our results to temperatures below the critical temperature, $T < T_c$. To properly incorporate the onset of the phase transition one could imagine going back through the work of sections 8.2-8.5 to incorporate anomalous contributions into the various propagator expansions. In fact, this is just what Kadanoff and Martin did [92] at the level of the Hartree-Fock approximation (for the nonresonant case), resulting in the conventional equations of BCS theory. The resulting t-matrix they found was the following:

$$t(Q) = -\frac{\Delta^2}{T}\delta(Q). \quad (8.36)$$

The singular nature of such a function leads us to think that it is this contribution to the t-matrix that dominates the onset of long-range order and that, perhaps, higher order anomalous contributions are negligible. We propose that the full scattering t-matrix should be composed of the BCS pairing interaction and an additional interaction which leads to non-condensed Cooper pairs:

$$t = t_{sc} + t_{pg}, \quad (8.37)$$

where t_{sc} is the superfluid condensate component and t_{pg} is the pseudogapped contribution. For the resonant system these may be defined as

$$t_{sc}(Q) = -\frac{\tilde{\Delta}_{sc}^2}{T}\delta(Q), \quad (8.38)$$

$$t_{pg}(Q) = \frac{g_{eff}(Q)}{1 + g_{eff}(Q)\chi(Q)}, \quad Q \neq 0. \quad (8.39)$$

Equation (8.38) is just a restatement of Eq. (8.36) for the resonant system and Eq. (8.39) comes from our $T > T_c$ result of the pseudogap process, Eq. (8.28). The effective, resonant interaction $g_{eff}(Q)$ is defined in Eq. (8.33) and the susceptibility $\chi(Q)$ is given by Eq. (8.34).

We identify the order parameter previously encountered in Chapter 5:

$$\tilde{\Delta}_{sc} = \Delta_{sc} - g\phi_m, \quad (8.40)$$

where $\phi_m = \langle b_{\mathbf{q}=0} \rangle$ is the condensed molecular component and $\Delta_{sc} = -U \sum_{\mathbf{k}} \langle a_{-\mathbf{k}\downarrow} a_{\mathbf{k}\uparrow} \rangle \varphi_{\mathbf{k}}$ is the standard BCS gap. The order parameter is a linear combination of both a pairing field and the closed-channel condensed molecules. It is, perhaps, enlightening to contrast this choice of an order parameter with the classic work of Fano on resonances [99]. For a potential resonance dominated by a bound state Fano chose the following ansatz for the wavefunction of eigenvalue E :

$$\Psi_E = a\varphi + \int dE' b_{E'} \psi_{E'}. \quad (8.41)$$

The above form is composed of a linear combination of a bound state φ and a range of continuum states $\psi_{E'}$ (a and b being constants). Fano found that this choice of wavefunction could be used to exactly solve the resonant problem. Although, strictly speaking, Eq. (8.41) is derived from a 2-body picture it shows a striking resemblance to the order parameter of Eq. (8.40).

It is worthwhile to write the order parameter, Eq. (8.40), in a form more closely resembling that of BCS theory. In Chapter 5.4 we found that the two components of the order parameter, ϕ and Δ_{sc} , are not independent, but are connected by the relation

$$\phi_m = \frac{g\Delta_{sc}}{(\nu - 2\mu)U}. \quad (8.42)$$

This implies that

$$\tilde{\Delta}_{sc} = -g_{eff}(0) \sum_{\mathbf{k}} \langle a_{-\mathbf{k}\downarrow} a_{\mathbf{k}\uparrow} \rangle \varphi_{\mathbf{k}}, \quad (8.43)$$

as one might expect.

8.8 Self-consistent equations for $T < T_c$

The form of the order parameter, Eq. (8.40), implies that the molecular bosons condense at the same temperature as a pairing field develops. Another way to state this would be:

$$D^{-1}(0) = t^{-1}(0) = 0, \quad T \leq T_c, \quad (8.44)$$

where D is the full bosonic Green's function. This statement simply relates the Thouless criterion to the criterion for Bose-Einstein condensation. Equation (8.44) leads to the important result:

$$t^{-1}(0) = g_{ef}^{-1}(0) + \chi(0) = 0, \quad T \leq T_c. \quad (8.45)$$

Equations (8.44) and (8.45) demand the following form for the bosonic self-energy:

$$\Sigma_B(Q) \equiv -g^2 \chi(Q) / [1 + U \chi(Q)], \quad (8.46)$$

which remains valid for $T \leq T_c$. Therefore, the full bosonic propagator is given by

$$D(Q) \equiv \frac{1}{i\Omega_n - E_q^0 - \nu + 2\mu - \Sigma_B(Q)}. \quad (8.47)$$

Equation (8.45) implies that t_{pg} is extremely sharp for all temperatures $T \leq T_c$. We may make use of the sharpness of the t-matrix to approximate Eq. (8.35) to yield a BCS-like self-energy

$$\Sigma(K) \approx -G_0(-K) \Delta^2 \varphi_{\mathbf{k}}^2, \quad (8.48)$$

with the following definition for the full gap:

$$\Delta^2 \equiv \tilde{\Delta}_{sc}^2 + \Delta_{pg}^2, \quad (8.49)$$

and where we have defined the pseudogap parameter Δ_{pg}

$$\Delta_{pg}^2 \equiv - \sum_{Q \neq 0} t_{pg}(Q). \quad (8.50)$$

For a more detailed discussion of the validity of this approximation see Maly *et al.* [100].

With these results, Eq. (8.45) can now be written as

$$g_{eff}^{-1}(0) + \sum_{\mathbf{k}} \frac{1 - 2f(E_{\mathbf{k}})}{2E_{\mathbf{k}}} \varphi_{\mathbf{k}}^2 = 0, \quad T \leq T_c, \quad (8.51)$$

where $E_{\mathbf{k}} = \sqrt{\epsilon_{\mathbf{k}}^2 + \Delta^2 \varphi_{\mathbf{k}}^2}$. Equation (8.51) is identical in form to the conventional BCS equation, but the full excitation gap Δ , as distinguished from the order parameter $\tilde{\Delta}_{sc}$, now appears in the dispersion $E_{\mathbf{k}}$.

To close these equations, we must now calculate the total particle number from the propagators involved. The number of molecular bosons is given directly by $n_b = -\sum_Q D(Q)$. The number of fermions is

$$n_f = \sum_{\mathbf{k}} \left[1 - \frac{\epsilon_{\mathbf{k}}}{E_{\mathbf{k}}} + 2 \frac{\epsilon_{\mathbf{k}}}{E_{\mathbf{k}}} f(E_{\mathbf{k}}) \right], \quad (8.52)$$

as follows from the condition $n_f = 2 \sum_K G(K)$. The total number N of particles is, therefore, given by

$$n_f + 2n_b + 2n_b^0 = N, \quad (8.53)$$

where $n_b^0 = \phi_m^2$ is the number of molecular bosons in the condensate. Equations (8.50), (8.51), and (8.53) form a closed set of equations for our resonance system. It should be noted that at $T = 0$ the pseudogap parameter, Eq. (8.50), vanishes ($\Delta_{pg} \rightarrow 0$) so that $\tilde{\Delta}_{sc}(0) = \Delta(0)$ and we reproduce BCS theory. In fact, one of the defining characteristics of this theory is that, at zero temperature, we reproduce the Leggett groundstate suggested in [81]. This would say that all the pseudogap behavior results from finite-temperature effects and at $T = 0$ the system is accurately described by conventional BCS theory.

An essential distinction between this and previous crossover studies based on the NSR approach [84, 101], below T_c , is that the modification to the energy spectrum is not fully accounted for by the superconducting gap, $\Delta \neq \tilde{\Delta}_{sc}$. This distinction, also absent in strict BCS theory, is to be associated with non-condensed bosonic excitations

of the superfluid. The spectrum of these excitations are modified due to the presence of other excitations. That is, the particles acquire a self-energy from other pairs present within the medium, which is fed back into the propagator for the pairs.

8.9 Numerical solution of the pseudogapped theory

We now numerically solve Eqs. (8.50), (8.51), and (8.53) for a homogeneous system. Although most atomic gas experiments are confined to a harmonic trapping potential, we don't expect the inhomogeneity of the trap to qualitatively alter the results we present here. To aid us in this task, we make use of the divergence of the t-matrix, expressed by Eq. (8.45). This allows us to Taylor expand the quantity $\chi(Q)$ in Eqs. (8.53) and (8.50) to first order in Ω and q^2 :

$$\chi(Q) \approx \chi(0) + a_0(i\Omega_n - B_0q^2). \quad (8.54)$$

We may expand $g_{eff}(Q)$ and $\Sigma_B(Q)$ in a similar fashion. These expansions considerably simplify the analysis (see Appendix E for a discussion of the expansion coefficients a_0 and B_0 and for a detailed discussion of implementing the pseudogap equations).

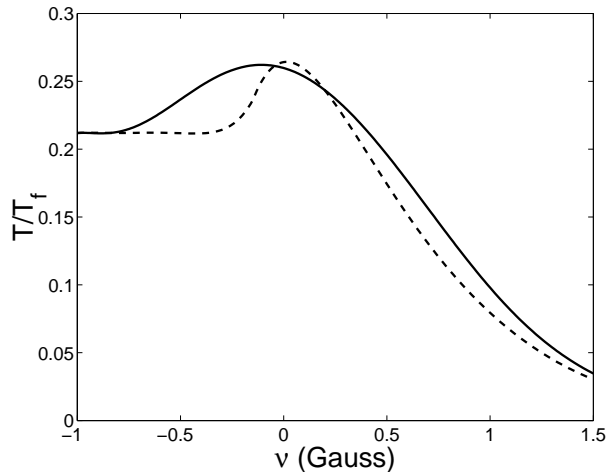


Figure 8.4: Comparison between the NSR approach (dashed line) and the pseudogap theory (solid line) for the critical temperature T_c/T_F of ^{40}K as a function of detuning ν . All parameters are chosen to be the same as those of Fig. 7.3.

We begin by comparing the results of the pseudogap theory to our earlier work of Chapter 7 where we analyzed the crossover for the case of ^{40}K . Figure 8.4 shows a direct comparison between the critical temperature prediction of the resonant NSR approach and the pseudogap equations we have just presented. With the inclusion of higher order corrections we still retain a pronounced maximum in T_c near the resonance at about $0.26T_F$.

To aid in illustrating the behavior of the resonant pseudogap equations we will leave the case of ^{40}K aside for a moment and instead explore a model atom more conducive to our discussion. We make this switch due to the positive value of the background scattering length in ^{40}K . This implies the presence of a bound state in the open channel which leads to an avoided crossing when the resonant molecular state is lowered well below threshold. Since we are not interested in this process, but would rather discuss the asymptotic case of a fully populated molecular fraction, we study a model atom with negative background scattering length. We choose $\bar{g}/E_F = -42$ and $\bar{U}/E_F = -3$ as indicative of currently trapped atomic Fermi gases. These parameters are, in fact, the same as those of ^{40}K , but we have flipped the sign of the background scattering length.

First we calculate T_c as a function of $\bar{\nu}$ which is plotted in Fig. 8.5. For $\bar{\nu} \rightarrow -\infty$, T_c approaches the ideal BEC limit. As $\bar{\nu} \rightarrow +\infty$, the bosonic populations become irrelevant and the asymptote of the curve is dictated by the behavior of the open channel fermions in the presence of the background interaction \bar{U} . It should be noted that in this work we have chosen a small \bar{U} deliberately so that $\bar{\nu} \rightarrow \infty$ limits to BCS theory. The figure indicates that, while there are differences in the shape of the T_c vs. $\bar{\nu}$ curve, the overall magnitudes are not so different from those found within our earlier NSR-based approach. More generally, we could contemplate a moderate value of \bar{U} where the asymptotic superfluid state will have a pseudogap. This might be relevant in the case of an atom such as ^6Li where the open channel contains a bound state close to

threshold leading to a large negative background scattering length, $a_{bg} \sim -2500a_0$.

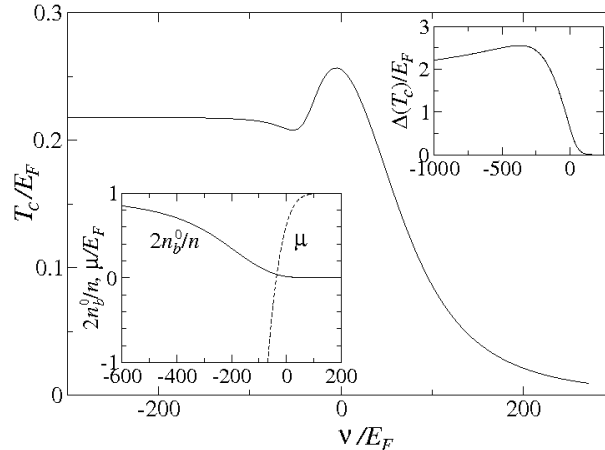


Figure 8.5: T_c vs. detuning ν with a pronounced maximum near threshold. The upper right inset plots the pseudogap at T_c vs. $\bar{\nu}$ with a maximum at large negative detuning. The lower left inset plots the molecular contribution to the condensate weight and the fermionic chemical potential.

Indicated as an inset in the figure is the behavior of $\Delta(T_c)$ as a function of $\bar{\nu}$. As $\bar{\nu}$ approaches the resonance from $+\infty$, T_c first increases following the BCS trend, which reflects an increasingly attractive pairing interaction. Likewise, the pseudogap, which starts at zero, begins to grow. At the point where the pseudogap becomes appreciable, the rise in T_c slows down. Eventually T_c decreases as fewer fermions are available to pair. An interesting feature of the pseudogap plot is that a maximum arises at large negative detuning. This behavior has not been witnessed in the non-resonant theory.

In the inset to Fig. 8.6, we plot the temperature dependence of the normalized excitation gap $\Delta(T)/\Delta(0)$ for three values of the detuning $\bar{\nu}/E_F = -200, -5, +200$. The middle value roughly corresponds to the maximum in T_c , where pseudogap effects should be the most apparent. The first and last are illustrative of the BEC and BCS limits, respectively. We, thus, refer below to these three values as the *BEC*, *PG*, and *BCS* cases. The order parameter, $\tilde{\Delta}_{sc}$, is not plotted here, but for all three cases it is rather close to the solid line in the inset. That $\Delta(T)$ is relatively constant with T

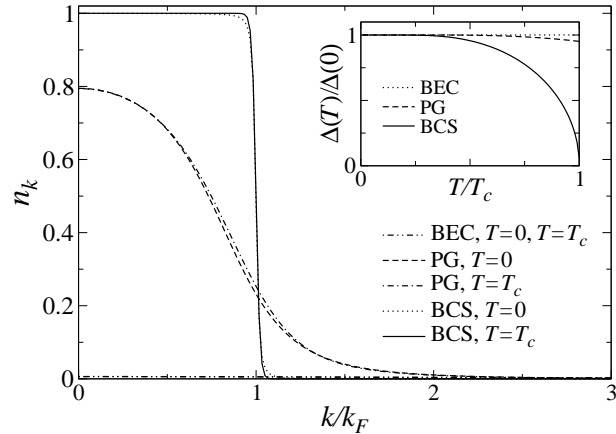


Figure 8.6: Fermionic momentum distribution function at $T = 0$ and $T = T_c$ for the three regimes. PG corresponds to maximal T_c . Inset plots the T dependent excitation gap below T_c .

through the superfluid transition is to be expected in the presence of preformed pairs, as we see for $\bar{\nu}/E_F = -5$ and -200 .

It should be stressed that the critical temperature T_c for the phase transition to superfluidity is only apparent in $\Delta(T)$ for the BCS case. To stress this point, in the body of Fig. 8.6, we plot the fermionic momentum distribution function n_k , which is the summand in Eq. (8.52):

$$n_k = \left[1 - \frac{\epsilon_{\mathbf{k}}}{E_{\mathbf{k}}} + 2 \frac{\epsilon_{\mathbf{k}}}{E_{\mathbf{k}}} f(E_{\mathbf{k}}) \right], \quad (8.55)$$

at $T = 0$ and $T = T_c$. From the figure, it is clear that there is very little temperature dependence between $T = 0$ and $T = T_c$. This is a clear sign that the momentum distribution is not a good indicator of phase coherent pairing [102]. For the PG case, where the critical temperature is a maximum, this results in the near temperature independence of $\Delta(T)$. In the far BEC limit the excitation gap does not vary at all through T_c . In the BCS regime, $\Delta(T)$ is so small as to be barely perceptible in the figure. In order to address the question of whether a clear signature can be seen in the particle density distribution [49, 60] these results must be generalized to a trapped system. A simple approach would be to treat the system under a local density approximation as

was done in Chapter 5.

This pseudogap based phenomenology is well documented in high- T_c superconductors. For these materials, penetration depth data provides a direct probe of the transition to superconductivity. Interestingly enough, densities of state measurements in the Cuprates also show some indications of the establishment of order throughout the sample. To see how phase coherence enters in the context of atomic physics, we relax the approximation of Eq. (8.48) by noting that incoherent, or finite momentum, pairs (pg) are distinguishable from coherent, or zero momentum, pairs (sc) through lifetime effects. The incoherent nature of the non-condensed pairs is affected by scattering events and therefore incorporates a finite broadening into the self-energy Σ_{pg} . With this intuition, the self-energy can be replaced by the model self-energy [95]:

$$\Sigma(\omega, \mathbf{k}) \approx \frac{\Delta_{pg}^2}{\omega + \epsilon_{\mathbf{k}} + i\gamma} + \frac{\tilde{\Delta}_{sc}^2}{\omega + \epsilon_{\mathbf{k}}}, \quad (8.56)$$

where γ is the finite broadening. We will not directly calculate γ , but will instead treat it as a phenomenological parameter which is independent of T . To calculate the density of states we remember that

$$G^{-1} = G_0^{-1} - \Sigma, \quad (8.57)$$

relates the self-energy Σ (in this case we use the form of Eq. (8.56)) to the full propagator G . The density of states, defined by [98]:

$$N(\omega) = -2 \sum_{\mathbf{k}} \text{Im} G(\omega + i0, \mathbf{k}), \quad (8.58)$$

can be directly evaluated given Eq. (8.56).

Figures 8.7(a)-8.7(c) show the results of evaluating Eq. (8.58), and correspond to the *BEC*, *PG*, and *BCS* cases displayed in the previous figures. The temperatures shown are taken just above T_c , $T = 0.75T_c$, and $T = 0.5T_c$. The *BCS* case is indicated by an abrupt transition at the critical temperature T_c . The density of states in the *BEC* regime shows very little temperature dependence throughout, since the fermions

are tightly bound into molecules at all temperatures. The *PG* case, which is taken near resonance at the point where T_c is a maximum, is the most interesting. A signature of superfluid order, seen by the presence of sharp coherence features, is not clearly perceptible until the temperature is well below the critical temperature. For the present case these features do not appear until a temperature of about $T = 0.5T_c$ is reached. However, the appearance of a pseudogap is clearly signalled by a suppression in the availability of low energy excitations displayed within the density of states plot. Similar observations to these are made in the high- T_c cuprates.

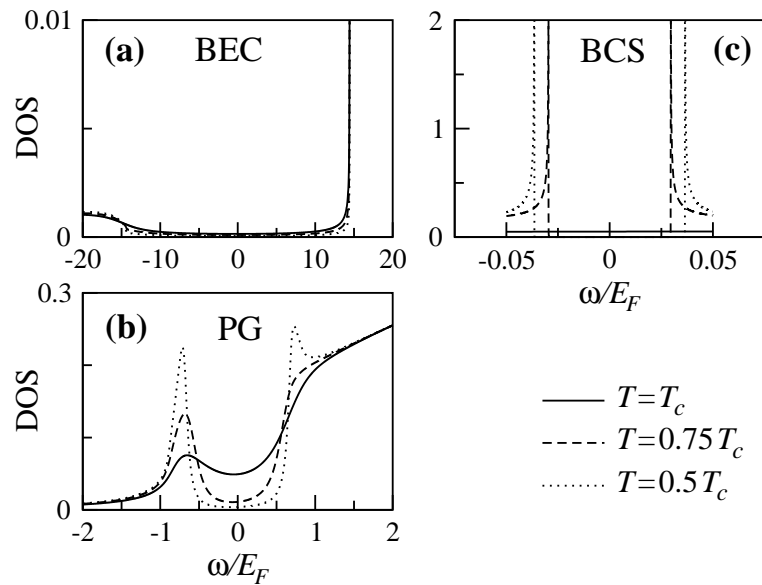


Figure 8.7: Fermionic density of states vs. energy for the three regimes at three indicated temperatures. Note the difference in the scales.

8.10 Conclusions and experimental implications

These plots have important implications for the interpretation of several predicted signatures of superfluidity. One such proposal is based on laser probing of “atomic Cooper pairs” where it has been argued that there is a conceptual analogy between normal metal-superconductor tunnelling (which measures $N(\omega)$), and the resonant scat-

tering of laser light [62]. The present work introduces a caution in interpreting future trapped atomic gas experiments. Because of the presence of a pseudogap, the signatures of superfluid onset are not as simple as in BCS or the related Bogoliubov-de Gennes theory. In general, one has to distinguish between the superfluid order parameter and the fermionic excitation gap. Nevertheless, superfluid coherence appears to be visible as fine structure effects in the fermionic density of states. While several experimentally accessible signatures, such as those displayed in the quantities $N(\omega)$ and n_k , do not provide a clear indication of superfluidity, they do establish the nature of the pairing regime as that of a pseudogapped superfluid.